Glacier Forecast: Jakobshavn Isbrae Primed for Thinning and Acceleration

Josh Willis (joshua.k.willis@jpl.nasa.gov)
Jet Propulsion Laboratory, California Institute of Technology https://orcid.org/0000-0002-4515-8771
Dustin Carroll
2Moss Landing Marine Laboratories, San José State University
Alex Gardner
Jet Propulsion Laboratory, California Institute of Technology https://orcid.org/0000-0002-8394-8889
Ala Khazendar
Jet Propulsion Laboratory, California Institute of Technology
Michael Wood
Jet Propulsion Laboratory, California Institute of Technology https://orcid.org/0000-0003-3074-7845
David Holland
3Courant Institute of Mathematical Sciences, New York University
Denise Holland
3Courant Institute of Mathematical Sciences, New York University
Ian Fenty
Jet Propulsion Lab
Eric Rignot
Jet Propulsion Laboratory, California Institute of Technology
Nolwenn Chauche
Access Arctic
Aqqalu Rosing-Asvid
Greenland Institute of Natural Resources

Article

Keywords: ocean climate, Jakobshavn Isbrae, sea-level rise, glacier forecasting

Posted Date: August 5th, 2020

DOI: https://doi.org/10.21203/rs.3.rs-51457/v1

Abstract

After three years of cold conditions, warm water has returned to Ilulissat Icefjord, home to Jakobshavn Isbrae—Greenland's largest outlet glacier. Jakobshavn has slowed and thickened since 2016, when waters near the glacier cooled from 3 °C to 1.5 °C. Fjord temperatures remained cold through at least the end of 2019, but in March 2020, temperatures in the fjord warmed to 2.8 °C. As a result of the warming, we forecast that Jakobshavn Isbrae will accelerate and resume thinning during the 2020 melt season. The fjord's profound influence on glacier behavior, and the connectivity between fjord conditions and regional ocean climate imply a degree of predictability that we aim to test with this forecast. Given the global importance of sea-level rise, we must advance our ability to forecast such rapidly changing systems, and this work represents an important first step in glacier forecasting.

1 Ocean-driven Changes In Jakobshavn Isbrae

By 2050, as many as 350 million people could be affected by the rising oceans (Kulp and Strauss, 2019). This makes predicting global sea-level rise one of the most urgent challenges for climate scientists. At present, the Greenland Ice-Sheet has 7.4 m of sea-level rise potential (Aschwanden et al., 2019; Morlighem et al., 2017). Projections of ice loss from Greenland during the 21st Century (Goelzer et al., 2020) rely on simplified, glacier-dependent relationships between the ocean and the outlet glaciers that drain the ice sheet (Slater et al., 2019a; 2019b). Yet it will take years, perhaps decades, to determine whether such simple assumptions will hold true in the future. Here we consider a seasonal forecast for the largest tidewater glacier in Greenland, Jakobshavn Isbrae, that can be tested within the next year. Although long-term projections remain the scientific goal, short-term forecasts like this one provide an opportunity to test the reliability of the underlying assumptions.

Jakobshavn Isbrae (known locally as Sermeq Kujalleq) is Greenland's largest glacier in terms of ice discharge and has been the focus of intense study for decades. After more than 20 years of flow acceleration and thinning, Jakobshavn Isbrae thickened and slowed each year from 2016 to 2019. This sudden change was driven by the arrival of cold water in Disko Bay during 2016, which was traced to a short-term cooling along Greenland's southwest coast (Khazendar et al., 2019). Based on those conclusions, Khazendar et al. (2019) suggested that warm water would return to Disko Bay in the near future, and hence speed up and thinning would resume.

Similar to previous short-term cooling events (Gladish et al., 2015a; 2015b), and the warming of late the 1990s (Holland et al., 2008), Khazendar et al. (2019) showed that glacier retreat, flow acceleration and thinning were all strongly correlated with the temperature of ocean waters that come in contact with the glacier front. More specifically, they found that glacier behavior was best explained by plume-driven melt rates at the glacier grounding line. These melting rates depend on both fjord temperature and the volume of meltwater discharge that flows along the glacier's bed during summer (Jenkins, 2011). In contrast, Joughin et al. (2020) suggested that fjord water temperatures affected the glacier by controlling the stiffness of the ice mélange that fills the fjord. This hypothesis suggests that during the winter, ice

mélange stiffens and exerts increased back-stress against the glacier front (Amundson et al., 2010; Cassotto et al., 2015). Both the plume-driven melt and ice mélange hypotheses affect glacier behavior by controlling the rate of calving or ablation at the glacier front. However, subglacial discharge occurs primarily in summer when runoff from the ice sheet is largest, and ice mélange stiffening occurs in winter when air temperatures are cold and sea ice grows. Regardless of the mechanism, it is increasingly clear that ocean temperatures play a major role in determining the frontal position, velocity, and thickness of Jakobshavn Isbrae (Bondzio et al., 2018).

As part of an ongoing effort to fill bathymetry gaps in key Greenlandic fjords, the University of California, Irvine conducted a short cruise through the western half of Ilulissat Icefjord between 29 March and 1 April 2020 (See Figure 1 for a view of the study area). During the cruise, three Conductivity-Temperature-Depth (CTD) profiles were collected along the main axis of the fjord. Combined with additional fjord observations since 2009, these profiles reveal the abrupt return of warm water after three years of cold conditions. A modest amount of thinning and acceleration at the glacier front has also been observed between March 2019 and spring 2020. However, our analysis shows that this thinning and acceleration occurred during the summer melt season of 2019, during a record year of ice-sheet surface melt (Velicogna et al, 2020; Tedesco and Fettweis, 2020). By the end of August 2019, surface melt on the ice sheet had largely subsided, but observations collected in the fjord at that time show the temperatures remained cold. Additional temperature data in the fjord shows that warm water arrived in Ilulissat Icefjord in March 2020, much too late to impact the glacier during the 2019 melt season.

Given that hydrographic conditions in the fjord can persist across several years (Gladish et al., 2015a), this gives us an opportunity to forecast the thinning and acceleration of Jakobshavn Isbrae for a year with warm water in the fjord and a range of typical subglacial discharge. Based on our analysis below, we predict a thinning of 11.4 ± 7.1 m $year^{-1}$ between March 2020 and March 2021 within 5 – 10 km of the front. Furthermore, at a position approximately 5 km upstream of the May 2019 front position, we predict peak summer velocities of 14.1 ± 2.1 km $year^{-1}$, and an acceleration of 2.8 ± 0.9 km $year^{-1}$ during the summer melt season of 2020.

2 Observations

2.2 Return of Warm Water: CTD Observations in Ilulissat Icefjord

Since 2009, eXpendable CTDs (XCTDs) have been used to survey the Ilulissat Icefjord. First presented in Gladish et al. (2015a), XCTD profiles were typically collected in June, July, or August, with 9 – 12 profiles spaced along the length of the fjord, near the center line. Updated through 2018, these observations provide a recent time series of temperature and salinity within Ilulissat Icefjord. Additionally, as part of the NASA Mission Oceans Melting Greenland (OMG: Fenty et al., 2016), two profiles were collected using Airborne eXpendable CTDs (AXCTDs) approximately halfway between the mouth of the fjord and the glacier front on 29 August 2019. During the 2020 cruise, three profiles were collected inside the main fjord between 29 March and April 2. The western most profile reached a depth of 600 m, while the other two

profiles reached 400 m (See Figure 1 inset). Taken together, these observations provide a time series extending from 2009 – 2020.

Figure 2 shows yearly temperature profiles within the fjord as a function of longitude. In every year except 2016, profiles within the fjord are almost identical, regardless of where in the fjord they were collected. This suggests that near-uniform conditions along the length of the fjord are present most of the time, consistent with the findings of Gladish et al. (2015a). This is further illustrated in Figure 3, which shows temperature and salinity profiles color coded by year.

Unlike other years, the 2016 XCTD survey conducted on the 4th and 6th of June, shows large gradients in temperature and salinity between the mouth of the fjord and the glacier front. Mooring data from Davis Strait (Khazendar et al., 2019) showed that the cold water arrived in the Strait on April 30th 2016 and that temperatures and salinities around 250 m in Disko Bay matched properties at the mooring (see their Figure S9). This means the cold water arrived in Davis Strait approximately 35 days before the 2016 XCTD survey in the fjord. Given the short timespan between these observations, and the strikingly large gradients along the fjord (Figure 2, “2016” panel), it is possible that the 2016 XCTD survey was conducted just after the cold water had traversed Disko Bay, and while it was still spilling over the sill into the fjord. This timing is further supported by additional profile data shown in the Supplementary Information.

The cold water that flooded the fjord in 2016 remained through 2019 (Figure 2). Below 500 m, water cooled from 3°C to approximately 1.5 °C. As shown in Figures 2 and 3, fjord temperatures remained cold at least until August 29th 2019, when the OMG profiles were collected. However, by 29 March 2020, the cruise observations show that warm water had returned. This means that the fjord warmed to roughly 2.8 °C between September 2019 and March 2020.

The arrival time of the warm water was determined more precisely using additional fjord profile data collected from ringed seals equipped with CTD data-loggers (see Boehme et al., 2009 for a more complete description). These data are typically available from late fall through spring, and observations show that the warm water did not return to the fjord until March of 2020 (see Supplementary Information and Supplementary Figures 1 – 3).

2.3 The Disko Bay-Fjord Connection

The sill at the mouth of the fjord strongly controls the properties of the water entering from Disko Bay. Khazendar et al. (2019) assumed that temperature and salinity in Disko Bay at the sill depth were communicated regularly into the fjord, as demonstrated by Gladish et al. (2015a) for the years before the cooling. We analyzed hydrographic data for Disko Bay (Figure 4) from CTD and AXCTD profiles collected as part of OMG since 2015 and from the ICES (2014) database prior to that. The ICES data includes hydrographic stations collected by the Greenland Institute of Natural Resources as part of its Standard Hydrographic Coastal Monitoring Program. During this period, 5 – 10 profiles are usually available within the red box shown in Figure 1. These were averaged together to generate the red line shown in Figure 4.

Figure 4 shows a comparison of all temperature observations below 500 m inside the fjord with Disko Bay temperatures at 240 m—the approximate sill depth. The results are not sensitive to the precise depth, however, since vertical temperature gradients in Disko Bay are small within 20 – 30 m above and below the sill depth. The close correspondence between fjord and Disko Bay temperatures shows that the signals observed in Disko Bay propagate into the fjord, where they come into direct contact with the glacier front that sits 700 – 900 m below sea level. This observation confirms earlier conclusions, which were based on shorter time series (Gladish et al., 2015a; Khazendar et al., 2019).

The 2020 CTD data from the fjord were collected at the end of March, while other years were collected between June and August. However, Gladish et al. (2015a) showed that the seasonal cycle of water temperature in the fjord at depths below 300 m is not larger than a few tenths of a degree Celsius. Thus, the arrival of 2.8 °C water in the fjord is likely the result of another interannual shift. This implies that fjord conditions can shift rapidly, but then persist for months to years. This is also consistent with the additional fjord profile data shown in the Supplementary Information. The fact that these conditions persist means that the fjord waters have ample time to affect the glacier's evolution. Furthermore, the close oceanographic connection between the fjord and Disko Bay provide a means to link observed dynamic changes in Jakobshavn to broader oceanographic conditions on the shelf and hence to regional ocean and atmospheric variability.

Despite the importance of the sill for regulating temperatures in the fjord, bathymetry on the eastern slope of the sill had not been mapped. During the March/April 2020 cruise, a multibeam echo sounder was used to map the depth of the central fjord from the sill to about 30 km east—about half of the distance from of the sill to the present-day front (Figure 1, inset).

The east side of the sill was mapped in detail for the first time. Although the deepest route across the sill remains the 245m saddle point at the northern edge, bathymetry on the eastern rise was significantly deeper, with steeper margins than prior interpolated estimates (Morlighem et al., 2017). This is consistent with the findings of Scheick et al. (2019), who inferred deeper seafloor depths just inside the sill based on the flotation height of grounded icebergs there. This new bathymetry also revealed a previously unknown channel on the eastern side of the fjord, running from south west to north east across the southern half of the sill. The channel cuts south of the shallow rise due west of the fjord, which was assumed by Schumann et al. (2012) to be the submarine continuation of a land spit at the southern part of the fjord mouth. Further east of the sill (more than 6 – 7 km), the fjord bottom was found to be remarkably flat, which we attribute to the piling of glacier sediments.

The large interannual variations of temperature and salinity in Disko Bay and Ilulissat Icefjord suggest that these waters are connected to broader regional climate signals. Using an ocean state estimate, Khazendar et al. (2019) linked the arrival of cold water in Disko Bay to pronounced cooling along Greenland's southwest coast during the previous winter. This differed from the assessment of the previous cooling in 2010 made by Gladish et al. (2015b), who attributed that event to an increase in water from Baffin Bay reaching onto the shelf. Rysgaard et al. (2020) suggested a similar mechanism for the

2016 cooling. However, if the unusual temperature structure of Ilulissat Icefjord observed in 2016 indicates that cold water was just arriving, it can be used to calculate an advective time scale based on the fact that this water arrived at the mooring in Disko Bay 35 days earlier. Following bathymetric contours, it is approximately 500 km from Davis Strait to Ilulissat Icefjord, which suggests an advective speed of approximately 16 cm s^{-1}. This is consistent with velocities typically observed at the slope along the eastern side of Davis Strait (Curry et al., 2014; Gladish et al., 2015b), and supports the hypothesis that the cold water was advected from Davis Strait as suggested by Khazendar et al. (2019). Regardless of the pathway, it appears that water in Disko Bay and the fjord is replaced episodically in large events, or shifts, that can happen rapidly. This suggests that the warm water observed in spring of this year will persist throughout the 2020 summer melt season, with major implications for Jakobshavn.

2.1 Thinning and Acceleration of Jakobshavn Isbrae in 2019

After the arrival of cold water in 2016, Jakobshavn Isbrae slowed, advanced and thickened (Khazendar et al., 2019; Joughin et al., 2020). During the 2019 summer melt season, however, Jakobshavn accelerated and thinned enough that yearly elevation change became negative for the first time in 4 years. Between March 2019 and March 2020, we observe a thinning of 7.6 meters between 3 – 15 km of the glacier front.

From 2016 through 2019, OMG collected yearly surveys of most marine terminating glaciers in Greenland using the high resolution (~3 meter) GLISTIN-A radar. After 2019, OMG did not collect GLISTIN data, as the launch of ICESat-2 (Markus et al., 2017) now provides elevation measurements with decimeter accuracy over the entire ice sheet (Smith et al., 2020). Although they are sparser geographically (3 km), the ICESat-2 data allow us to estimate time series of glacier elevation, provided we consider a large enough area (Figure 5). The highest thinning rates at Jakobshavn occurred in the fastest moving ice and near the front, and decreased upstream as expected from dynamic thinning. It was also concentrated during the summer months, when glacier flow, surface melt, subglacial discharge—and hence, plume-driven melt—are all at their highest. Nevertheless, the timing of the 2019 thinning and acceleration show that they cannot be explained by the arrival of warm water in the fjord, which did not occur until March of 2020 (See Supplemental Information).

In addition to thinning, summer acceleration of Jakobshavn Isbrae was also observed in 2019 (Figures 6 and 7). After 3 years of lower peak velocities, and little acceleration during summer melt seasons, 2019 saw a return of vigorous acceleration and higher summer velocities. Similar to the thinning discussed above, these changes were coincident with summer ice sheet melt and subglacial discharge (Figure 7), as is typical during summer months.

Near the front, flow speeds increased from approximately 6.4 km $year^{-1}$ to more than 9.5 km $year^{-1}$, while upstream they increased from 5.6 to 7.7 km $year^{-1}$ (Figure 7). The larger increase near the front suggests longitudinal stretching, which is consistent with the thinning shown in Figure 5. After the summer speed-up, winter speeds from January through March of 2020 were similar to the same months during 2019 and 2018.

Seasonal acceleration and thinning happen in most years, and they coincide closely with the arrival of subglacial discharge, peaking in June or July. This is illustrated for the recent years in Figure 7, which shows both glacier speed and subglacial, plume-driven submarine melting. As described in Methods, plume-driven melt is a function of both fjord temperature and the rate of subglacial discharge. In every year since 2009 (when velocity observations became frequent enough to resolve the seasonal cycle), summer acceleration coincides with—or closely follows—increased daily rates of plume-driven melt. In 2009, plume-driven melt was higher, not because of warmer fjord temperatures, but because of record surface melt across the ice sheet and high rates of subglacial discharge. All of the thinning and acceleration in 2019 occurred before warm water returned to Ilulissat Icefjord.

3 Discussion And Hindcast Of 2019 Melt Season

The 2019 summertime thinning and acceleration of Jakobshavn cannot be explained by the return of warm water to the fjord. However, surface melt on the ice sheet was exceptionally high across all of Greenland in summer 2019. Surface melt over the drainage basin for Jakobshavn peaked in early August and had largely subsided by the end of the month, when the two OMG fjord profiles were collected showing that cold conditions had persisted throughout the summer and into March 2020. Therefore, we suggest that the thinning and acceleration of Jakobshavn Isbrae during 2019 was primarily caused by enhanced submarine melting of the glacier face driven by high subglacial discharge. Additionally, since warm water returned the fjord before the 2020 melt season began, we further hypothesize that rapid thinning, large acceleration, and high peak velocities will all return to Jakobshavn during summer 2020.

To test the predictability of these quantities, we first attempt to hindcast the glacier behavior in 2019 based on summer melt, velocities, and thinning rates from 2006 to 2018. Khazendar et al. (2019) used the summer mean of daily maximum melt rate values based on a one-dimensional, idealized plume model (Jenkins 2011; Carroll et al., 2016). The maximum melt rate usually occurs within ~100 m of the sea floor depth and is used as an indicator of undercutting and calving. While the absolute values of the plume melt rate are sensitive to details of the submarine melt parameterization, the year to year fluctuations are driven primarily by changes in fjord temperature and subglacial discharge, and it is from these interannual changes that we expect predictability for the glacier.

As for Khazendar et al. (2019), we find a strong linear relationship between the average summer maximum submarine melt rate and the amount of thinning each year (see Methods for calculation of thinning rates). Since elevation data was collected prior to the melt season during spring of each year, the change from one spring to the next was compared with the intervening summer melt season (Figure 8). The regression coefficient was -0.81, with a p-value of 0.0005. Although the relationship between plume-driven melt and thinning is strong, the RMS of the residuals for the least squares fit to the linear model was 7 m. Nevertheless, this uncertainty remains smaller than many of the ~15 – 30 m per year thinning and thickening rates observed in recent years. Based on the 2019 simulated summer melt rate of 7.2 m, the linear model suggests +0.8 m of thickening. While this is substantially different than the observed

-7.6 m of thinning (Figure 5), it is nevertheless significantly lower than the previous three years, which saw roughly 14 m of thickening.

As illustrated in Figure 7, summer velocities respond strongly to the rate of plume-driven submarine melt. Since 2008, satellite observations have become frequent enough to resolve the seasonal cycle of glacier velocities. We found that from 2008 through 2018, velocities were most closely related to peak summer melt rates, defined as the highest average melt rate in a 12-day period within each melt season. While glacier velocities were correlated with average summer melt rates as well, regression coefficients were consistently higher when using maximum summer melt rates.

Linear regressions between maximum summer melt rate and both peak summer velocity and summer speedup were calculated for the downstream point shown in Figure 5A. The summer speed up was defined as the increase in velocity between 1 May and 1 July for each year. This corresponds closely with the onset of the surface melt season and had the highest correlation coefficient ($r = 0.82$, with a p-value of 0.0034) of any relationship considered in this analysis. This is not unexpected as the onset of subglacial discharge, and hence plume-driven melt, clearly coincides with summer increases in velocity, and peak melt rates typically happen in early July.

Peak velocities were generally captured by the linear regression, with linear model suggesting a 2019 peak velocity of 11.6 km year^{-1} and an observed velocity of 9.8 km year^{-1}. The summer acceleration, however, was somewhat larger than predicted by the regression, with observed velocities increasing by 1.8 km year^{-1}, as opposed to the 1.2 km year^{-1} acceleration that was predicted. This is well within the range of RMS residuals for both estimates, where were 2.1 km year^{-1} for peak velocity and 0.94 km year^{-1} for summer speed up.

It is also possible to use these linear regression models to estimate how the 2019 melt year might have proceeded, had the warm water observed in March 2020 been present during the summer melt season. To do so, the plume model was re-run for 2019 using the temperature and salinity profiles observed in 2020. Based on the resulting melt rates, our linear regression models predict a thinning of 15.2 m, a peak velocity of 15.3 km year^{-1}, and a summer acceleration of 3.39 km year^{-1}, had warm water been present in 2019. The all three esimates differ sharply from the observed 2019 values. Although crude, these linear regression models appear to have at least some predictive skill. In terms of elevation change and peak summer velocity and summer speedup, they are consistent with cold conditions persisting in the fjord through all of 2019.

4 Forecast Of 2020 Thinning, Peak Velocity, And Summer Acceleration

Although warm water has returned to Ilulissat Icefjord, we have shown that the 2019 thinning and acceleration of Jakobshavn Isbrae was likely driven by enhanced submarine melt during summer, while the fjord waters were still relatively cold. Based on the March/April fjord observations, the warm water

has clearly returned but has not yet impacted the glacier. This provides a unique opportunity to test our understanding of the mechanism driving dynamic glacier change. Using the linear relationships derived above, we are able to forecast thinning, peak summer velocity and summer acceleration of Jakobshavn Isbrae expected during the 2020 melt season.

To create the forecast, we include the results of the 2019 observations and recalculate the linear regressions. The additional year made no significant changes to the linear fit, regression coefficients or p-values for estimated changes.

To account for uncertainty in the amount of subglacial runoff during the 2020 melt season, we consider the extreme high melt (2019) and low melt (2008) years of the previous two decades. Plume-driven melt for 2020 was estimated using the plume model (described in Methods) using the late March 2020 temperature and salinity profiles, and the upper and lower bounds years for subglacial discharge. We note that the RMS residuals to the fit provide a much larger uncertainty bound than the high and low discharge cases (Table 1). We therefore use the residuals as our uncertainty bound for the forecast. Based on these calculations, we predict thinning of 11.4 ± 7.1 m, 5 – 10 km upstream from the front, between March 2020 and March 2021. We also predict peak summer velocities of 14.4 ± 2.1 km year^{-1} in 2021, and an acceleration of 2.8 ± 0.9 km year^{-1} between May 1 and July 1 2020 at the location of the purple star in Figure 5A.

2020 Forecast for Jakobshavn Isbrae

	Elevation Change (m)	Peak Summer Velocity (km year^{-1})	Summer Acceleration (km year^{-1})
Low discharge (2008)	-7.8	13.2	2.25
High discharge (2019)	-15	15.1	3.33
Central Estimate	-11.4	14.1	2.79
RMS Residual	7.1	2.1	0.9

Table 1. Forecast for Jakobshavn Isbrae during the 2020 summer melt season. Elevation change represents an estimate of elevation differences from 10 – 15 km upstream of the front between March 2020 and March 2021. Peak summer velocity is an estimate of the maximum velocity at the point of the purple star shown in Figure 5A during 2020. Summer acceleration is an estimate of increased velocity between May 1 and July 1 2020. The high discharge year was taken to be 2019, and low discharge is 2008. The central estimate is considered the forecast and the RMS residuals provide an estimate of the uncertainty.

To be a true forecast, this estimate should ideally be made in advance of the 2020 melt season, which as of this writing has already begun. However, since peak melt rates often occur during August and observations of ice velocity and thickness have a latency of several months, we feel that this forecast can provide value to the community. Even if the forecast fails, it can provide insight—possibly exposing new mechanisms that drive glacier behavior or even ruling out proposed ones. At the very least it should server as a springboard for validating much needed projections of future sea level rise.

Methods

Ice Elevation Measurements

OMG's elevation data were collected using the GLISTIN-A radar (Khazendar et al., 2019). Three parallel swaths, each approximately 10 km in width and just over 100 km long were collected along the glacier, with a horizontal spatial resolution of 3 m. Uncertainties in the elevations measured by GLISTIN-A are estimated to be 1 – 2 meters (Moller et al. 2019). Data was collected in March of 2016, 2017, 2018, and 2019. A recent Level 3 gridded product was used, which places data from all survey years on a common, 50 m resolution grid (OMG, 2020).

The ICESat-2 Alt06 product was obtained from the National Snow and Ice Data Center (NSIDC, https://nsidc.org/data/atl06, Smith et al 2019) and gridded onto a 50 m regular grid using a nearest neighbor approach for comparison with the GLISTIN-A product. Data filtered by removing all ICESat-2 observations that differed by more than 30 m from the 2019 GLISTIN-A elevation map at the same location. This eliminated approximately 0.1% of ICESat-2 observations. The glacier center line shown in Figure 5A was based on the 2017 flight line from Operation IceBridge that was used as a reference track by Khazendar et al. (2019). Distance upstream from the 2020 glacier front was calculated using this line. The comparison region shown in Figure 5B was chosen by selecting all points within 2.5 km north and south of the line at every longitude and from 3 km to 15 km upstream of the 2019 front. The region begins 3 km upstream of the front to avoid front migration during the season.

Yearly Elevation Changes

For 2019 and 2020, thinning was detected by comparing elevations the ICESat-2 satellite with elevations from the 2019 OMG GLISTIN-A survey. Elevation data within a 2.5 km range of the centerline of the glacier, and between 3 and 15 km upstream from the front was used to compute the difference at various times, when ICESat-2 data was available. The 3 – 15 km range was chosen to allow for more data ICESat-2 data availability. For consistency with Khazendar et al. (2019), 10 – 15 km range upstream from the front was also computed. This reduced the amount of available ICESat-2 observations by approximately half and increased uncertainties, but did not affect the amplitude or timing of the observed elevation change signal, which was estimated to be -7.6 m between the date of the 2019 GLISTIN-A survey and exactly one year later.

For elevation changes from 2006 through 2017, the estimates of Khazendar et al. (2019) were used (see their Supplementary Table 1, normalized values). For changes from 2017 to 2018 and 2018 to 2019, the GLISTIN-A survey were used to calculate elevation changes from 10 – 15 km upstream of the front, and within 2.5 km of the glacier centerline shown in Figure 5A. These were found to be increases of 14.2 m from 2017 to 2018 and 14.4 m from 2018 to 2019. For consistency with the 2019/2020 comparison using ICESat-2, the average between 3 – 15 km was also considered for these years and found to be 15.8 m and 15.0 m, respectively. These values are slightly higher since they contain elevation changes closer to the front. However, such differences are not much larger than expected uncertainties (~1 m, Moller et al., 2019), and they make no significant difference to the hindcast or forecast calculations. This suggests that comparison of these elevation changes to the broader search region used for the 2019 comparison

with ICESat-2 should pose no problem with consistency across the different types of elevation estimates.

Uncertainty in ICESat-2 Minus GLISTIN-A Elevation Changes

ICESat-2 observations are irregular in time and space over Jakobshavn. However, GLISTIN-A data provide complete coverage of glacier elevations collected in a single day. To estimate how well ICESat-2 data observe the elevation change in the average over the region inside the green contour shown in Figure 5B, we subsampled the elevation changes based on GLISTIN for the changes between 2016 to 2017, 2017 to 2018, and 2018 to 2019. The root mean square of the subsampled estimate relative to the “true” change calculated from the full GLISTIN-A maps was taken to be the uncertainty in the estimate of mean change shown in Figure 5B.

Velocity Measurements

Surface velocities are derived from feature tracking of repeat optical imagery (Landsat 4, 5, 7 and 8; and Sentinel-1a/b and -2a/b) using autonomous Repeat Image Feature Tracking (autoRIFT: Gardner et al., 2018). Velocities are generated for all image pairs with <65 days of separation and have uncorrelated errors of ~30 – 300 m $year^{-1}$. Velocities were also extracted from NASA’s MEaSUREs Greenland Ice Velocity data set (Joughin et al., 2010) derived from TerraSAR-X and Sentinel-1 a/b image pairs and have an uncorrelated uncertainty of ~5 – 20 m $year^{-1}$.

Glacier Front Melt Rates

Using observations of Jakobshavn grounding line depth and fjord hydrography, it is possible to model an idealized subglacial plume and compute glacier melt rates (Jenkins 2011; Carroll et al., 2016). Here we follow a similar approach to Khazendar et al. (2019) to compute a time series of plume-driven glacier melt rates from 2004–2020. For 2004–2009, when fjord hydrography was not available, we assume that water properties at the glacier terminus are equal those in Disko Bay for depths <= 250-m deep sill. Below that depth, temperature and salinity are assumed to be homogenous. To estimate subglacial discharge, we use 20-km daily surface runoff from MAR 3.11, scaled by elevation area within the catchment basin using the 150 m resolution surface elevation estimate from GIMP (Howat et al., 2014). Subglacial discharge is computed over a probability-based catchment area that is delineated by a Monte Carlo-based approach (Carroll et al., 2016); here we used the maximum catchment size. Plume-driven melt rates also have a small dependence on the depth of the glacier, although for the range of depths occupied by Jakobshavn during this analysis, depth dependence is very small. Nevertheless, annual estimates of grounding line depth are based on bed depths from BedMachine Version 3, and front positions were estimated using Landsat 7 and 8 imagery from 5 June 2018, 7 May 2019, and 7 May 2020. These dates were chosen for consistency with Khazendar et al. (2019, see their Supplementary Table 1). As done in Khazendar et al. (2019), we ignore plume-driven melting when discharge is less than 1 m^3 s^{-1} and use the maximum melt rate above the grounding line (see Fried et al., 2015; Rignot et al., 2015).

Acknowledgments And Data

The research described in this paper was carried out at the Jet Propulsion Laboratory, California Institute of Technology, under a contract with NASA. There are no financial conflicts of interest for any authors, or conflicts due to their affiliations. Oceanographic profiles, ice elevation and bathymetry data collected as part of the OMG mission can be obtained from https://omg.jpl.nasa.gov/. Additional oceanographic profile data from Disko Bay were identified using a combination of in situ CTD measurements from the International Council for the Exploration of the Sea Oceanography Data Portal (http://www.ices.dk/) and the World Ocean Database. Glacier velocity data was provided by the NASA MEaSUREs ITS_LIVE (Gardner et al., 2019: https://its-live.jpl.nasa.gov/) and GIMP (Joughin et al., 2010: https://nsidc.org/data/nsidc-0481) projects.

The authors thank the Greenland Institute of Natural Resources, Nuuk Greenland, for collection of hydrographic data in Disko Bay as part of its Standard Hydrographic Coastal Monitoring Program. ICESat-2 data are available at https://nsidc.org/data/atl06. DH and DMH acknowledge support from grant G1204 of NYU Abu Dhabi's Center for global Sea Level Change and NSF grant ARC-1304137.

Seal tagging was conducted under the general permit of Greenland Institute of Natural Resources issued by the Greenland Government: Anon. (2010) "Selvstyrets bekendtgørelse nr. 16 af 12. november 2010 om beskyttelse og fangst af sæler" [The Greenland Government executive order no. 16, dated 12. November 2010 about protection and hunting of seals]. Seal data is available from the NSF Arctic Data Center (https://arcticdata.io/catalog/view/doi:10.18739/A2NV99B1S).

References

Amundson, J. M., Fahnestock, M., Truffer, M., Brown, J., Lüthi, M. P., and Motyka, R. J. (2010),Ice mélange dynamics and implications for terminus stability, Jakobshavn Isbræ, Greenland, *J. Geophys. Res.*, 115, F01005, doi:10.1029/2009JF001405.

Aschwanden, A., Fahnestock, M. A., Truffer, M., Brinkerhoff, D. J., Hock, R., Khroulev, C., et al. (2019), Contribution of the Greenland Ice Sheet to sea level over the next millennium. *Sci. Adv.*, 5(6), eaav9396. https://doi.org/10.1126/sciadv.aav9396.

Boehme, L., Lovell, P., Biuw, M., Roquet, F., Nicholson, J., Thorpe, S. E., Meredith, M. P., and Fedak, M. (2009), Technical Note: Animal-borne CTD-Satellite Relay Data Loggers for real-time oceanographic data collection, *Ocean Sci.*, *5*, 685–695, https://doi.org/10.5194/os-5-685-2009.

Bondzio, J. H., Morlighem, M., Seroussi, H., Wood, M., & Mouginot, J. (2018), Control of ocean temperature on Jakobshavn Isbræ's present and future mass loss. *Geophys. Res. Lett.*, 45, 12,912–12,921. https://doi.org/10.1029/2018GL079827

Carroll, D. et al. (2016), The impact of glacier geometry on meltwater plume structure and submarine melt in Greenland fjords. *Geophys. Res. Lett.*, *43*, 9739–9748, https://doi.org/10.1002/2016GL070170.

Cassotto, R., Fahnestock, M., Amundson, J., Truffer, M., & Joughin, I. (2015). Seasonal and interannual variations in ice melange and its impact on terminus stability, Jakobshavn Isbræ, Greenland. *J. Glaciol.*, 61(225), 76-88. doi:10.3189/2015JoG13J235

Curry, B., C. M. Lee, B. Petrie, R. E. Moritz, and R. Kwok, 2014: Multiyear Volume, Liquid Freshwater, and Sea Ice Transports through Davis Strait, 2004–10. *J. Phys. Oceanogr.*, 44, 1244–1266, https://doi.org/10.1175/JPO-D-13-0177.1.

Fenty, I., Willis, J. K., Khazendar, A., DiNardo, S., Forsberg, R., Fukumori, I., et al. (2016), Oceans melting Greenland: Early results from NASA's ocean–ice mission in Greenland. *Oceanography*, *29*(4), 72–83, https://doi.org/10.5670/oceanog.2016.100.

Fried, M. J., G.A. Catania, T. C. Bartholomaus, D. Duncan,M. Davis, L. A. Stearns, J. Nash, E. Shroyer, and D. Sutherland (2015), Distributed subglacial discharge drives significant submarine melt at a Greenland tidewater glacier, *Geophys. Res. Lett.*, *42*, 9328–9336, doi:10.1002/2015GL065806.

Gardner, A. S., M. A. Fahnestock, and T. A. Scambos, (2019), ITS_LIVE Regional Glacier and Ice Sheet Surface Velocities. Data archived at National Snow and Ice Data Center; [data accessed: 22 July 2020], doi:10.5067/6II6VW8LLWJ7.

Gardner, A. et al. (2018), Increased West Antarctic and unchanged East Antarctic ice discharge over the last 7 years, *Cryosphere*, *12*, 521–547.

Gladish, C. V., Holland, D. M., and Lee, C. M (2015a), Oceanic Boundary Conditions for Jakobshavn Glacier. Part II: Provenance and Sources of Variability of Disko Bay and Ilulissat Icefjord Waters, 1990–2011, *J. Phys. Oceanogr.*, *45*, 33–63, https://doi.org/10.1175/JPO-D-14-0045.1.

Gladish, C. V., Holland, D. M., Rosing-Asvid, A., Behrens, J. W., and Boje, J. (2015b), Oceanic Boundary Conditions for Jakobshavn Glacier. Part I: Variability and Renewal of Ilulissat Icefjord Waters, 2001–14, *J. Phys. Oceanogr.*, *45*, 3–32, https://doi.org/10.1175/JPO-D-14-0044.1.

Howat, I. M., A. Negrete, B. E. Smith (2014), The Greenland Ice Mapping Project (GIMP) land classification and surface elevation data sets, *Cryosph. 8*, 1509–1518, https://doi.org/10.5194/tc-8-1509-2014, 2014.

Holland, D. M., Thomas, R. H., De Young, B., Ribergaard, M. H., and Lyberth, B (2008), Acceleration of Jakobshavn Isbrae triggered by warm subsurface ocean waters, *Nat. Geosci.*, *1*, 659–664, https://doi.org/10.1038/ngeo316.

ICES (2014), Dataset on Ocean Hydrography, The International Council for the Exploration of the Sea, Copenhagen, Extractions 31-August 2018, Disko Bay Ocean Temperature Data collected by the Greenland Institute of Natural Resources (GL). ICES, Copenhagen.

Jenkins, A. (2011), Convection-driven melting near the grounding lines of ice shelves and tidewater glaciers, *J. Phys. Oceanogr.*, *41*, 2279–2294, https://doi.org/10.1175/JPO-D-11-03.1.

Joughin, I., Shean, D. E., Smith, B. E., and Floricioiu, D, (2020), A decade of variability on Jakobshavn Isbræ: ocean temperatures pace speed through influence on mélange rigidity, *The Cryosphere*, *14*, 211–227. https://doi.org/10.5194/tc-14-211-2020.

Joughin, I., Smith, B., Howat, I., Scambos, T. & Moon, T. (2010), Greenland flow variability from ice-sheet-wide velocity mapping. *J. Glaciol.*, *56*, 415–430, https://doi.org/10.3189/002214310792447734.

Khazendar, A., Fenty, I. G., Carroll, D., Gardner, A., Lee, C. M., Fukumori, I., Wang, O., Zhang, H., Seroussi, H., Moller, D., Noel, B. P. Y., Van Den Broeke, M. R., DiNardo, S., and Willis, J., (2019), Interruption of two decades of Jakobshavn Isbrae acceleration and thinning as regional ocean cools, *Nat. Geosci.*, *12*, 277–283, https://doi.org/10.1038/s41561-019-0329-3.

Kulp, S.A., Strauss, B.H. (2019), New elevation data triple estimates of global vulnerability to sea-level rise and coastal flooding, *Nat. Commun.*, *10*, 4844 (2019), https://doi.org/10.1038/s41467-019-12808-z.

T. Markus, et al. (2017), The Ice, Cloud, and land Elevation Satellite-2 (ICESat-2): Science requirements, concept, and implementation. *Remote Sens. Environ.*, *190*, doi:10.1016/j.rse.2016.12.029.

Moller, D., Hensley, S., Mouginot, J., Willis, J., Wu, X., Larsen, C., Rignot, E., Muellerschoen, R., Khazendar (2019), A. Validation of Glacier Topographic Acquisitions from an Airborne Single-Pass Interferometer. *Sensors*, *19*(17), 3700. https://doi.org/10.3390/s19173700.

Morlighem, M., et al. (2017), BedMachine v3: Complete Bed Topography and Ocean Bathymetry Mapping of Greenland From Multibeam Echo Sounding Combined With Mass Conservation, *Geophys. Res. Lett.*, *44*, 11051–11061, https://doi.org/10.1002/2017GL074954.

OMG (2020), OMG Mission: Glacier elevation data from the GLISTIN-A campaigns. ver. 1. PO.DAAC, CA, USA. Dataset accessed [2020-Jul-03], https://doi.org/10.5067/OMGEV-GLNA1.

Rignot, E., I. Fenty, Y. Xu, C. Cai, and C. Kemp (2015), Undercutting of marine-terminating glaciers in West Greenland, *Geophys. Res. Lett.*, *42*, 5909–5917, doi:10.1002/2015GL064236.

Rysgaard, S., Boone, W., Carlson, D., Sejr, M. K., Bendtsen, J., Juul-Pedersen, T., et al. (2020), An updated view on water masses on the pan-west Greenland continental shelf and their link to proglacial fjords. J*ournal of Geophysical Research: Oceans*, *125*, e2019JC015564. https://doi.org/10.1029/2019JC015564.

Scheick, J., Enderlin, E., Miller, E., Hamilton, G (2019), First-Order Estimates of Coastal Bathymetry in Ilulissat and Naajarsuit Fjords, Greenland, from Remotely Sensed Iceberg Observations. *Remote Sens.*, *11*, 935, http://dx.doi.org/10.3390/rs11080935.

Schumann, K., Völker, D., Weinrebe, W.R (2012), Acoustic mapping of the Ilulissat Ice Fjord mouth, West Greenland, *Quat. Sci. Rev.*, *40*, 78–88, https://dx.doi.org/10.3390/rs11080935.

Slater, D. A., Felikson, D., Straneo, F., Goelzer, H., Little, C. M., Morlighem, M., Fettweis, X., and Nowicki, S. (2019a), 21st century ocean forcing of the Greenland Ice Sheet for modeling of sea level contribution, *The Cryosphere Discuss.*, *2019*, 1-34, doi:10.5194/tc-2019-222.

Slater, D. A., Straneo, F., Felikson, D., Little, C. M., Goelzer, H., Fettweis, X., and Holte, J. (2019b), Estimating Greenland tidewater glacier retreat driven by submarine melting, *The Cryosphere*, 13, 2489-2509, doi:10.5194/tc-13-2489-2019.

Smith, B., H. A. Fricker, N. Holschuh, A. S. Gardner, S. Adusumilli, K. M. Brunt, B. Csatho, K. Harbeck, A. Huth, T. Neumann, J. Nilsson, M. R. Siegfried (2019), Land ice height-retrieval algorithm for NASA's ICESat-2 photon-counting laser altimeter. *Remote Sens. Environ.*, 111352, https://doi.org/10.1016/j.rse.2019.111352.

Smith et al. (2020), Pervasive ice sheet mass loss reflects competing ocean and atmosphere processes, *Science*, *368*(6496), 1239-1242, https://doi.org/10.1126/science.aaz5845.

Tedesco, M., and X. Fettweis (2020), Unprecedented atmospheric conditions (1948-2019) drive the 2019 exceptional melting season over the Greenland ice sheet. *The Cryosphere*, *14*, 1209-1223, doi:10.5194/tc-14-1209-2020.

Velicogna, I., Mohajerani, Y., A, G., Landerer, F., Mouginot, J., Noel, B., et al. (2020). Continuity of ice sheet mass loss in Greenland and Antarctica from the GRACE and GRACE Follow-On missions. *Geophysical Research Letters*, *47*, e2020GL087291, https://doi.org/10.1029/2020GL087291

Figures

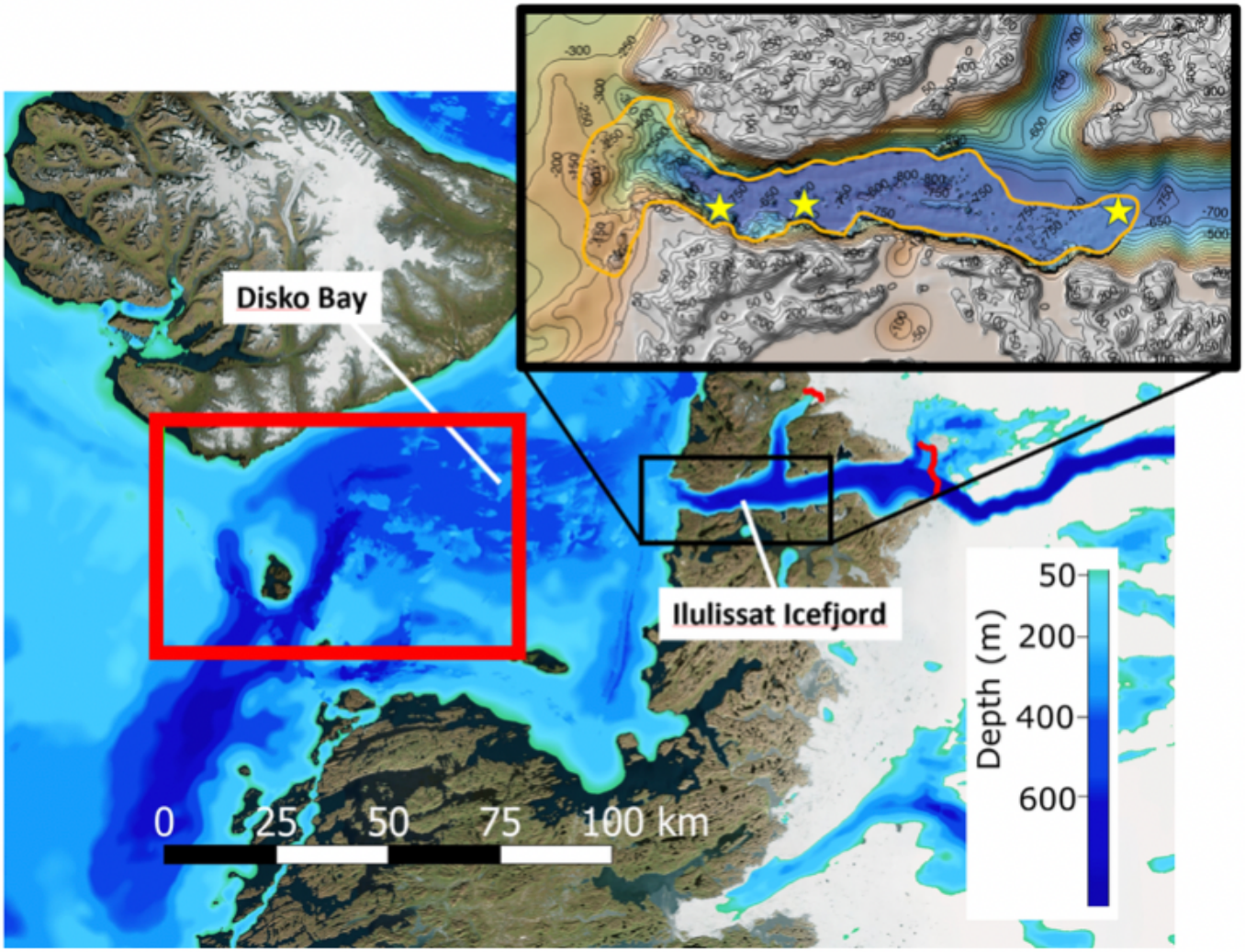

Figure 1

Ocean depth (bathymetry) in Disko Bay and Ilulissat Icefjord. The inset shows multibeam echo sounding-derived fjord bathymetry from the 2020 cruise with sharp valley boundaries and a flat fjord bottom. Stars mark the locations of the 3 CTD profiles collected. The orange line delimits the approximate extent of the multibeam echo sounder data. The red box shows the region within which Disko Bay temperature profiles are averaged to provide a proxy for fjord temperatures, as in Khazendar et al. (2019). The red lines in the fjord show the approximate position of the glacier front in 2017.

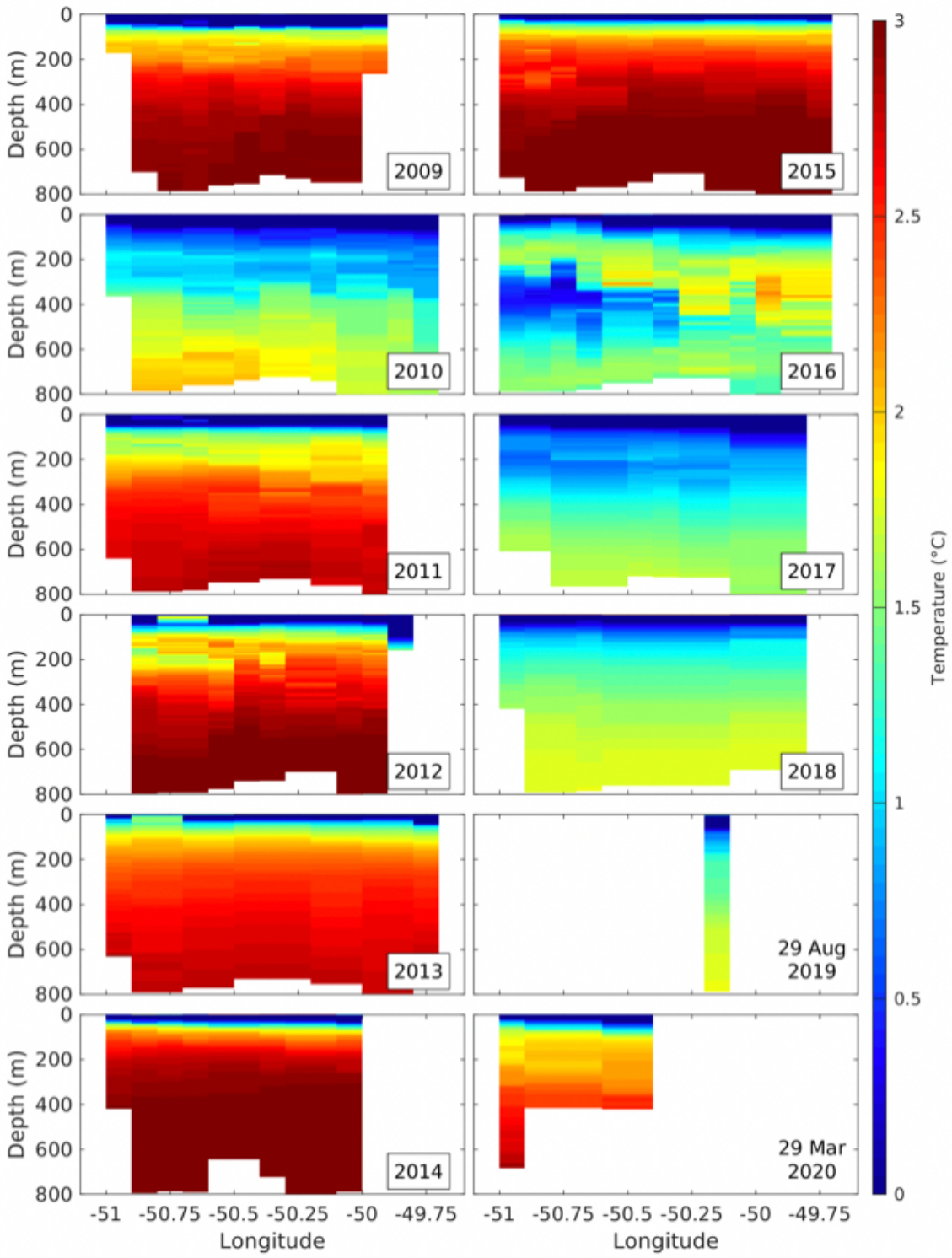

Figure 2

Temperature sections along the centerline of Ilulissat Icefjord as a function of depth and longitude. Note the short-term cooling in 2010 reported by Gladish et al. (2015a; 2015b) and arrival of cold water in 2016. Only two profiles in 2019 were collected by OMG on 29 August. The three profiles collected during the 2020 cruise show the return of warm water in the fjord. The eastern edge of the plots is close to the glacier front position of recent years.

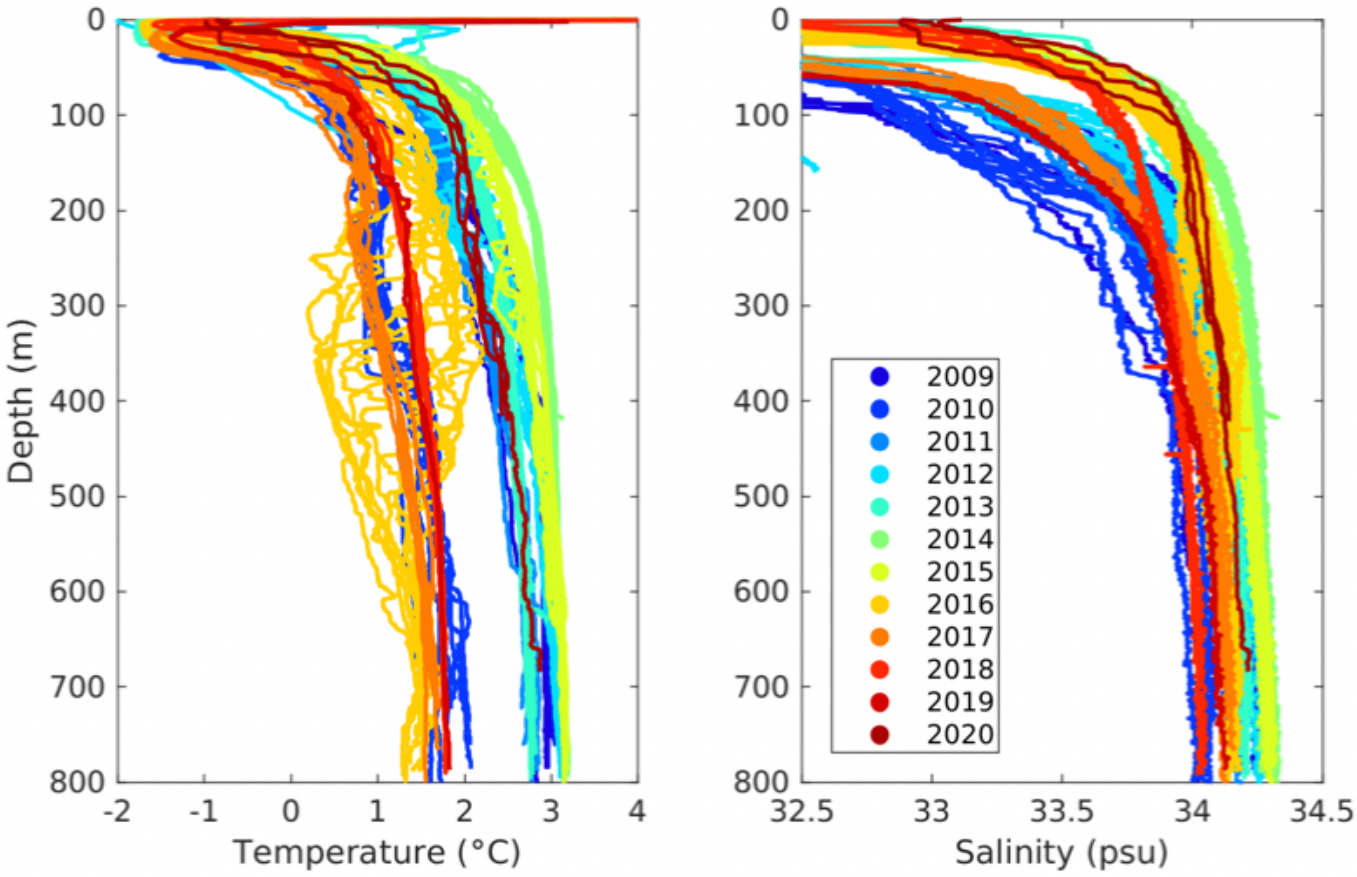

Figure 3

Temperature (left) and salinity (right) profiles from Figure 2, color coded by year. Except for 2016, all years show tightly-grouped profiles in both temperature and salinity, reflecting the relatively uniform temperature and salinity structure within the fjord. The return of warm water before April 2020 is illustrated by the dark red profiles of 3 °C water atop the clusters of warm profiles from 2015 and earlier.

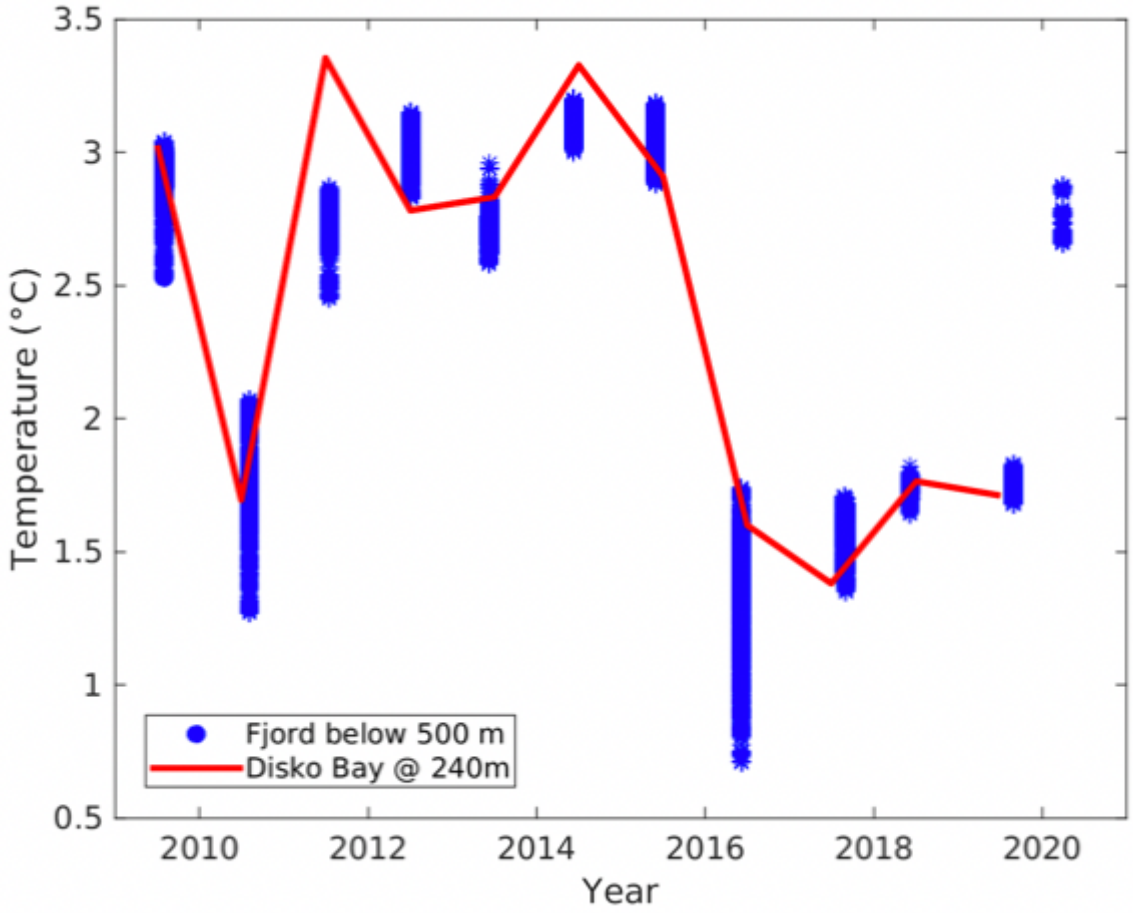

Figure 4

Temperature at 240 m in Disko Bay (red line) from data collected within the red box shown in Figure 1, compared with temperatures below 500 m from within Ilulissat Icefjord.

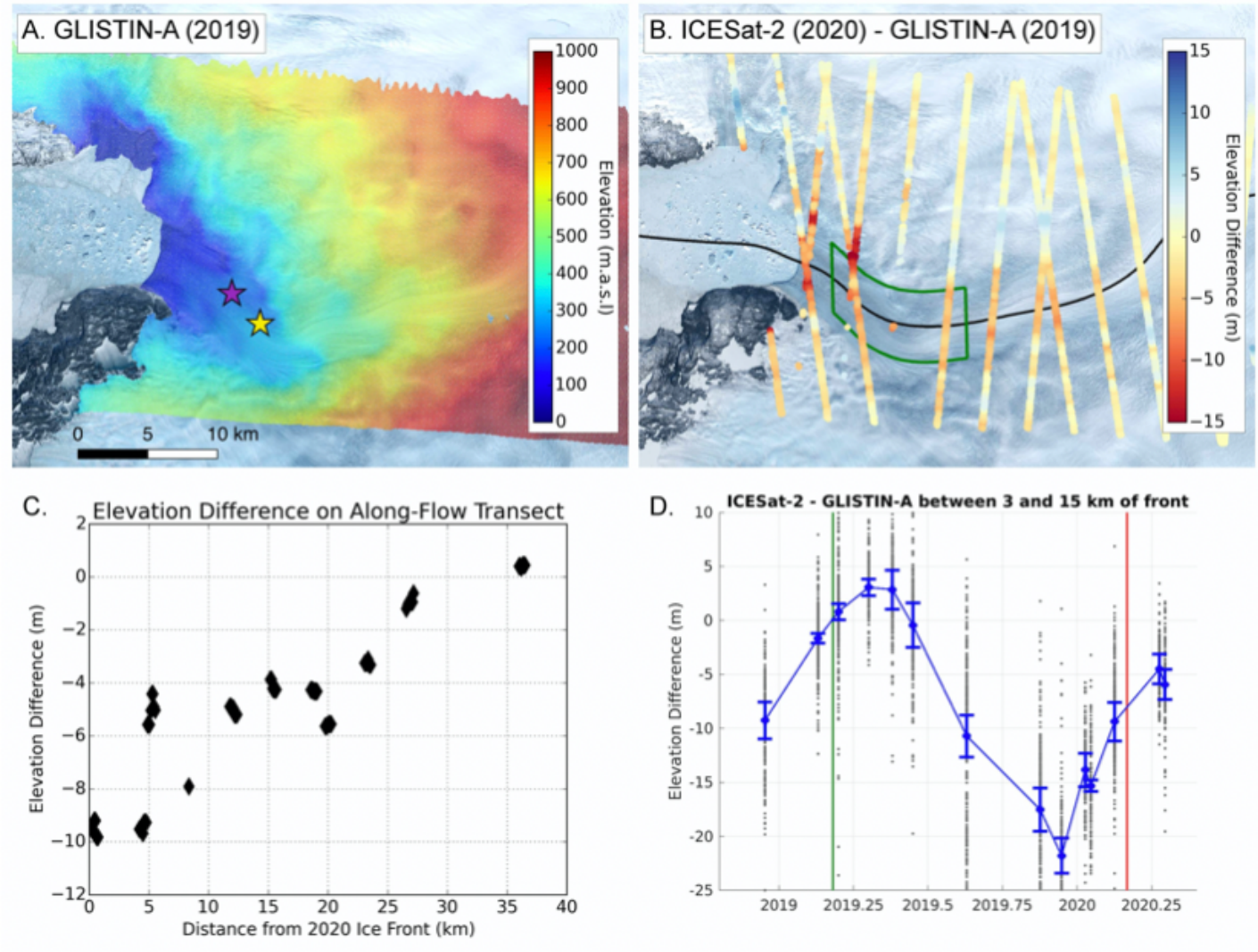

Figure 5

A. 2019 elevation data over Jakobshavn Isbrae from GLISTIN-A. Purple and Yellow stars show the locations of velocity observations in Figure 7, approximately 5 and 8 km upstream of the May 2019 front position, respectively. B. The difference between elevations from GLISTIN-A (date from Mar 2019) and ICESat-2 (data from Mar – April 2020). C. Elevation differences within 2.5 km of the glacier center line (black line in B). D. Mean elevation differences between ICESat-2 and GLISTIN-A over the region between 3 – 15 km upstream of the May 2019 front and within 2.5 km of the center line (green contour in B). Grey dots show individual measurements, blue dots show the mean. Errors bars represent sampling uncertainty, calculated as described in Methods. The green line shows the timing of the GLISTIN-A survey. The red line shows the arrival of the warm water in March 2020. Most of the thinning occurred in summer months. The background images in A and B are “natural” color Landsat-8 scenes of the glacier from April 2019 and 2020, respectively.

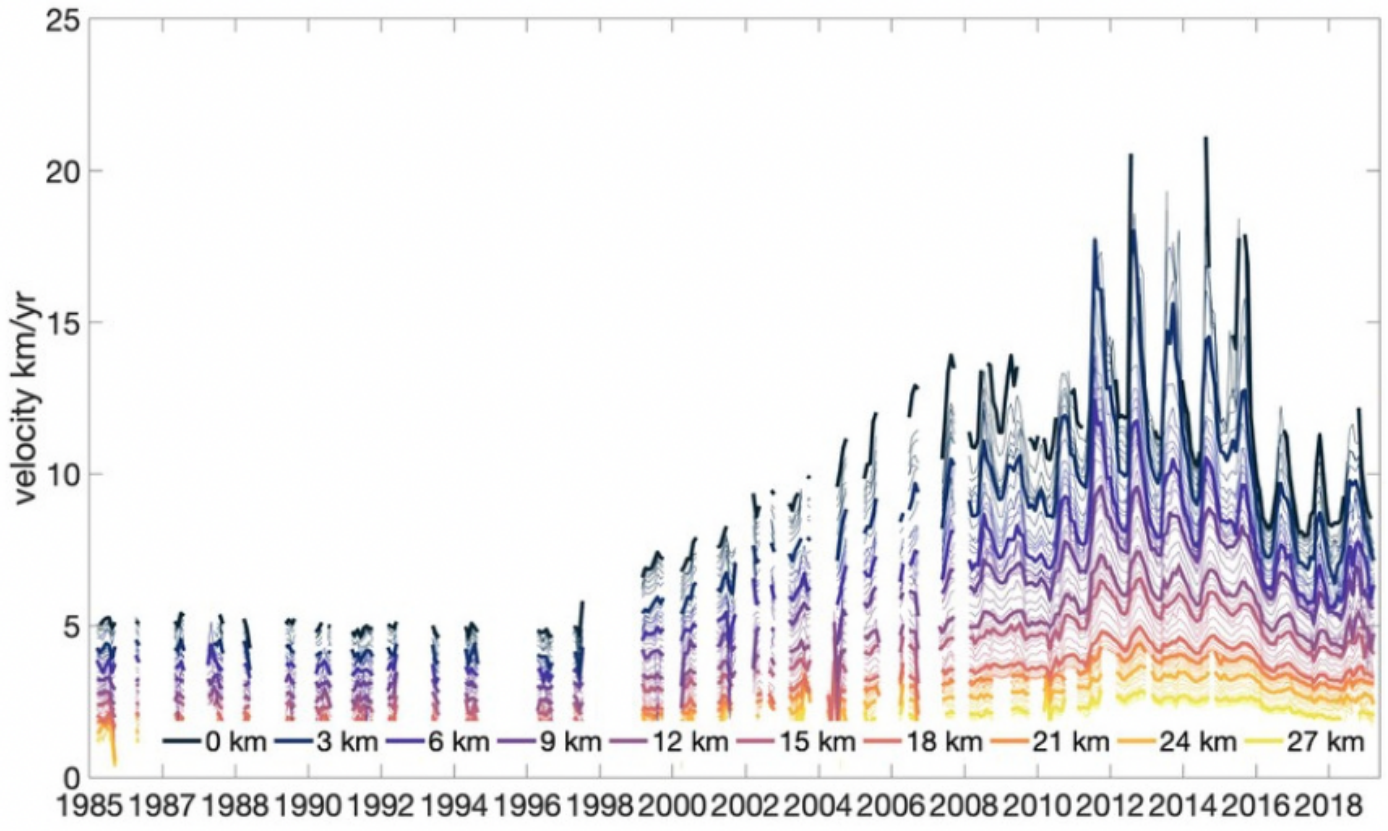

Figure 6

Glacier flow speed (velocity) at various points along the Jakobshavn Isbrae centerline. Speeds are highest near the front (purples) and decrease upstream (yellows). Speeds slowed after the arrival of cold water in summer of 2016 and accelerated again in 2019.

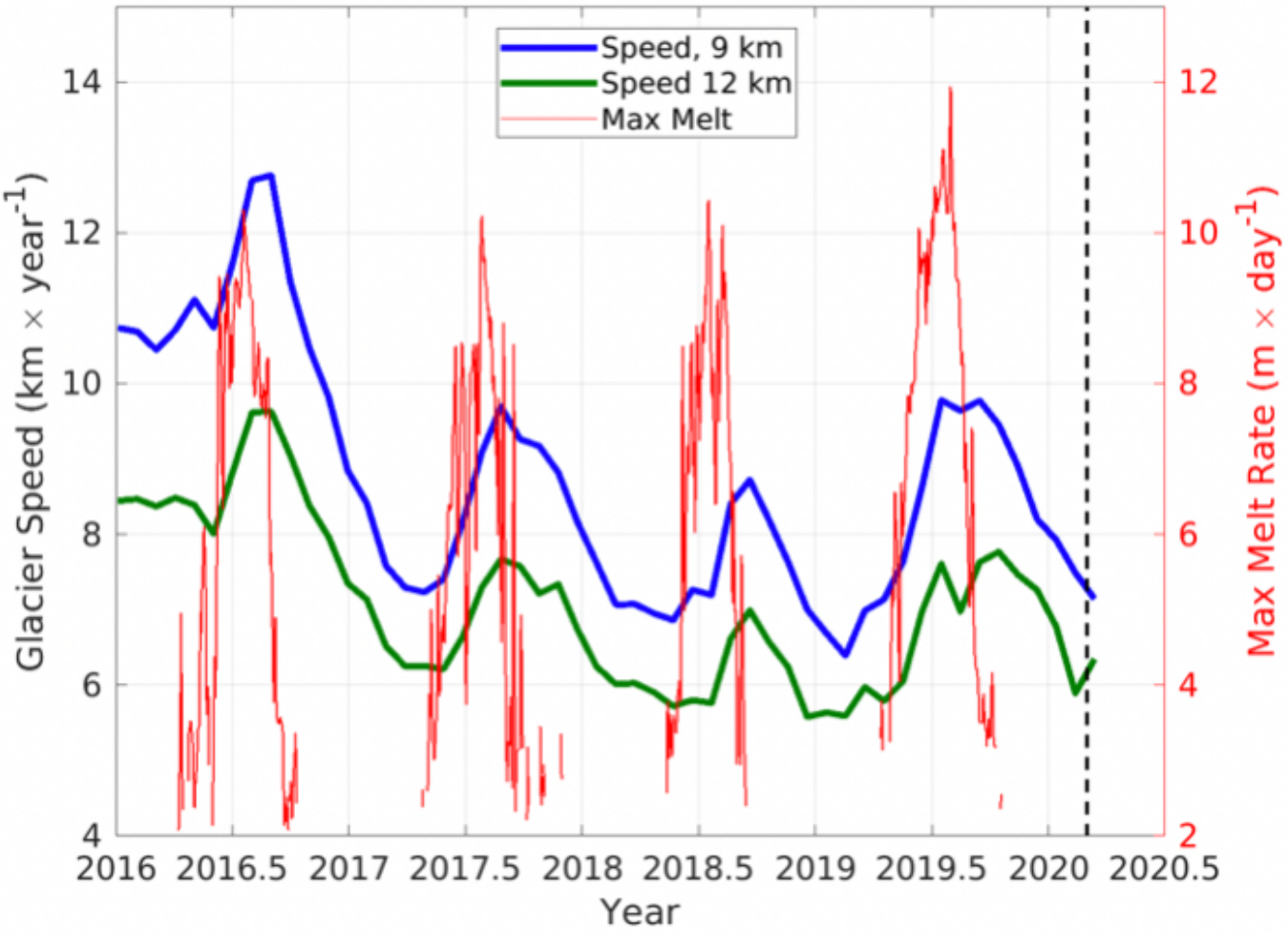

Figure 7

Glacier flow speed at 5 (Figure 5A, purple star) and 8 km (Figure 5A, yellow star) from the front for 2016 – 2020, along with daily maximum summer melt rates (calculated as described in Methods). Note that plume-driven melt rates are significant only during June, July and, August when subglacial discharge is present, and are always coincident with the summer glacier acceleration. The dashed vertical line shows the approximate time when warm water returned to the fjord (See Supplemental Information).

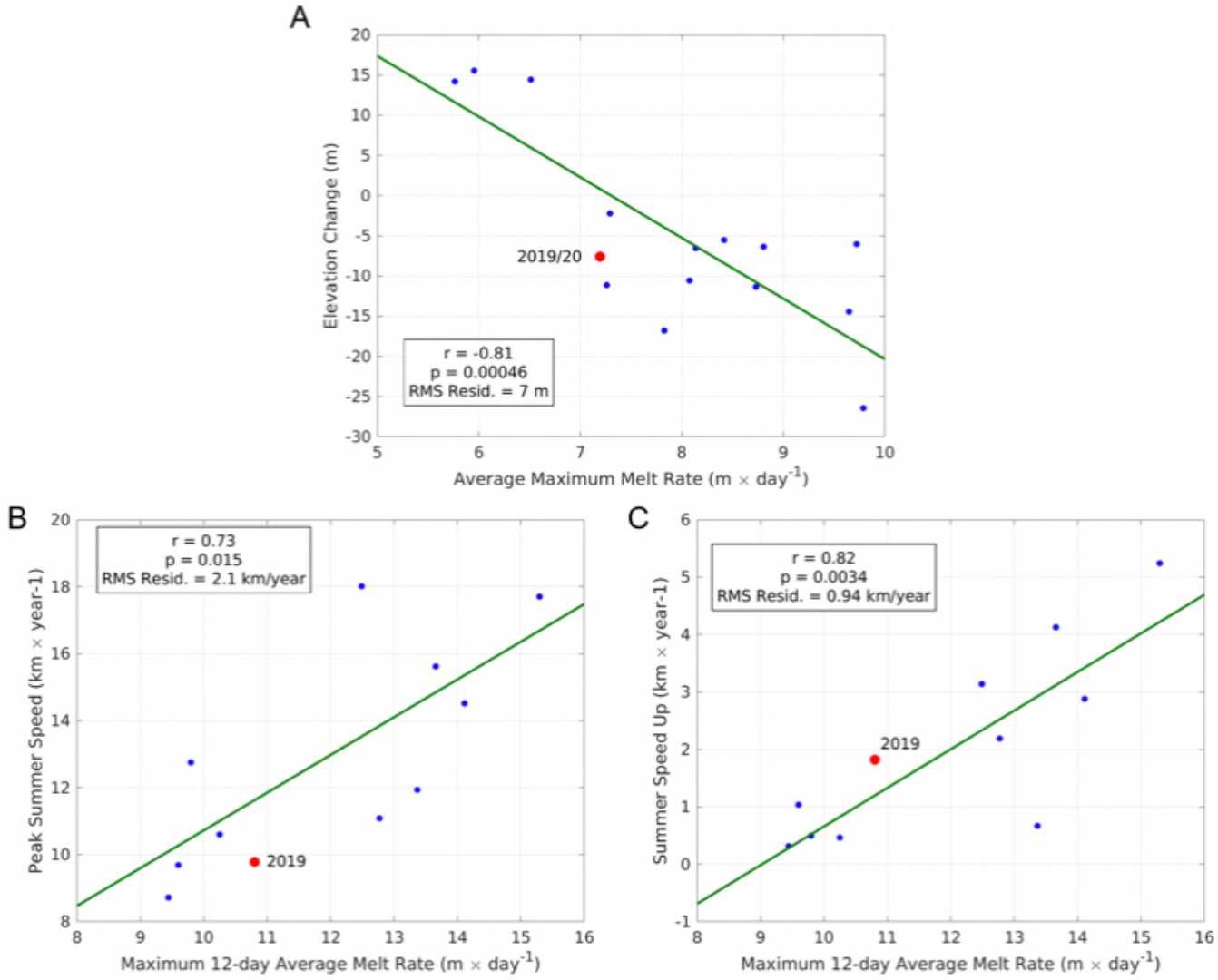

Figure 8

A. Linear regression of glacier elevation changes onto melt rate. B. Regression of maximum summer velocity at the downstream point shown in Figure 5A onto maximum summer melt rate. C. Regression of glacier velocity change at the downstream point between May 1 and July 1 onto maximum summer melt rate. In all panels, the red dot shows the observations in 2019 (or the 2019 – 2020 change in A), which was excluded from the regression calculation.

Supplementary Files

This is a list of supplementary files associated with this preprint. Click to download.

- WillisJakForecastSupplement.docx